Journal of Applied Physics

Magnetic and electronic structures of antiferromagnetic topological material candidate $EuMg_2Bi_2$

Cite as: J. Appl. Phys. **129**, 035106 (2021); https://doi.org/10.1063/5.0035703
Submitted: 30 October 2020 . Accepted: 28 December 2020 . Published Online: 19 January 2021

Madalynn Marshall, Ivo Pletikosić, Mohammad Yahyavi, Hung-Ju Tien, Tay-Rong Chang, Huibo Cao, and Weiwei Xie

Journal of Applied Physics ARTICLE scitation.org/journal/jap

Magnetic and electronic structures of antiferromagnetic topological material candidate $EuMg_2Bi_2$

Cite as: J. Appl. Phys. **129**, 035106 (2021); doi: 10.1063/5.0035703
Submitted: 30 October 2020 · Accepted: 28 December 2020 ·
Published Online: 19 January 2021

View Online Export Citation CrossMark

Madalynn Marshall,[1,2] Ivo Pletikosić,[3] Mohammad Yahyavi,[4] Hung-Ju Tien,[4] Tay-Rong Chang,[4,5] Huibo Cao,[2,a)] and Weiwei Xie[1,a)]

AFFILIATIONS

[1]Department of Chemistry and Chemical Biology, Rutgers University, Piscataway, New Jersey 08854, USA
[2]Neutron Scattering Division, Oak Ridge National Laboratory, Oak Ridge, Tennessee 37831, USA
[3]Department of Chemistry, Princeton University, Princeton, New Jersey 08540, USA
[4]Department of Physics, National Cheng Kung University, Tainan 70101, Taiwan
[5]Center for Quantum Frontiers of Research and Technology (QFort), Tainan 70101, Taiwan

Note: This paper is part of the Special Topic on Topological Materials and Devices.
a)Authors to whom correspondence should be addressed: caoh@ornl.gov and weiwei.xie@rutgers.edu

ABSTRACT

$EuMg_2Bi_2$ has been investigated to understand the electronic and magnetic behaviors as an antiferromagnetic (AFM) topological semimetal candidate. High-quality single crystals of $EuMg_2Bi_2$ were grown via a Bi flux and, subsequently, characterized to be consistent with the previously reported bulk magnetic and resistivity properties. A ferromagnetic interaction is indicated by the positive Curie–Weiss temperature obtained through fitting the bulk magnetic susceptibility data. The bulk resistivity measurements reveal an interesting electronic behavior that is potentially influenced by a competing antiferromagnetic and ferromagnetic interaction in and out of the *ab* plane. From the resulting refinement of the neutron diffraction data, $EuMg_2Bi_2$ was found to exhibit an A-type magnetic structure with Eu^{2+} moments ferromagnetically aligned in the plane and antiferromagnetically stacked between neighbor ferromagnetic Eu layers. The power law fitting magnetic ordering parameter below $T_N \sim 8$ K agrees with the 2D Heisenberg model, indicating a weak interlayer antiferromagnetic interaction. Considering the magnetic structure determined by neutron diffraction, the surface state calculation suggests that $EuMg_2Bi_2$ is an AFM topological insulator candidate. Linearly dispersed Dirac surface states were also observed in our angle-resolved photoemission spectroscopy measurements, consistent with the calculation.

INTRODUCTION

Since the discovery of Dirac fermions in graphene, interest in topological materials has accelerated along with the complexity of newly uncovered exotic electronic structures. Topologically protected electronic surface states in Dirac materials are distinctive from the bulk states and can be characterized by the linear energy-momentum dispersion near the Fermi level and massless chiral excitations of their electrons.[1] Recently, the focus has shifted from topological insulators (TIs) to topological semimetals (TSMs). Driving these materials even further, we can incorporate additional quantum phases such as superconductivity, magnetism, and charge density waves into the host material possessing the topological electronic surface states to explore the new physics that arises.[2,3] With the addition of magnetism in the TSM condensed matter, scientists have realized materials that can host nontrivial phenomena such as axion electrodynamics, the quantum anomalous Hall effect (QAHE), and Majorana fermions.[4–6]

Magnetic TSMs have the potential to be used in a range of applications including spintronics and optical devices as heterogeneous catalysts.[7,8] One such avenue being photonics and nonlinear optics applications where recent advances have shown that 3D Dirac semimetals can generate extreme THz harmonics, such as in

Cd_3As_2.[9–11] TMSs have also been considered for electronic devices, including Na_3Bi that was discovered to be a high-efficiency electrical contact material for 2D semiconductors.[12] Emerging TSM-based electronic devices have included ultrafast broadband photodetectors and spin topological field effect transistors.[13] However, the stability, cost, and ease of fabrication are crucial factors that must be taken into account if magnetic TSMs are to become technologically relevant today. Topological materials such as $(Bi,Sb)_2Te_3$,[14] which have been magnetically doped as thin films, often produce sharp inhomogeneities; therefore, intrinsic magnetic topological materials provide a more reliable platform. In order to discover new intrinsic magnetic TSMs, attention must be directed to the current chemical factors that have proven to drive band inversion. This includes chemical bonding, spin–orbit coupling (SOC), nuclear and magnetic structure and symmetry, etc.[15,16] In the TSM Na_3Bi,[17,18] the formation of the Dirac nodes is based on the energetically low 6*s* Bi orbitals and a SOC. A similar dependency is also observed in the low-lying energy 5*s* Cd orbitals of the tetragonal Dirac semimetal Cd_3As_2.[19] A chemical bonding motif that has proven to produce an even greater band inversion energy than in Na_3Bi and Cd_3As_2 is the 4^4 square net.[20] The epitome of the square net motif is exhibited in the TSMs found in the PbFCl structural family, such as ZrSiS,[21] and in $AMnBi_2$ (A = alkaline-earth-metal).[22] Likewise, the ABX honeycomb structure (ZrBeSi-type, space group P63/mmc; No. 194) has been reported to vary in its topological properties as a direct result of an interplay between the atomic orbitals and ionic sizes present in the local structures (i.e., $X[B_3A_6]$).[23]

After the band inversion has been considered, the next action is to incorporate the magnetic component, and an excellent platform for this is through rare earth elements, which can promote the coupling between topological quasiparticles and magnetism. Within the $XMnBi_2$ (X = rare earth elements) family, which acquires a Bi square net motif, various topological candidates have been discovered including $EuMnBi_2$;[24–26] a TSM candidate shown to exhibit phenomena such as the half-integer Quantum Hall effect and magnetopiezoelectric properties. Additionally, antiferromagnetic (AFM) $YbMnBi_2$[27,28] has been suspected to host Weyl fermions, the formation of which is believed to be dependent on the ∼10° spin canting of the Mn moments. Such an observation, resultantly, reveals the influence that magnetism has on controlling the electronic surface states. Subsequently, the layered triangular lattice compound $EuCd_2As_2$[29] has been identified as an AFM Dirac semimetal candidate. The triangular layers of ferromagnetic (FM) Eu moments provide a rich playing field for diverse magnetic behavior and interactions.

Mg_3Bi_2[30] was recently discovered by Chang *et al.* as a potential type-II nodal-line semimetal. The strong SOC from Bi in Mg_3Bi_2 combined with the weak interlayer interactions and a partial confinement of the electronic states has promoted the formation of topological states. Subsequent investigations into this structure type may potentially reveal a new motif for magnetic topological semimetals. Considering the potential interplay between the topological electronic states and magnetism with the replacement of one equivalent of Mg in Mg_3Bi_2 with one equivalent of magnetic Eu, we found interest in investigating $EuMg_2Bi_2$.[8,31,32] The previously reported semimetal $EuMg_2Bi_2$, isostructural to $EuCd_2As_2$ sharing the space group *P*-3m1 (no. 164), was found to be a topological candidate with an AFM behavior, $T_N \sim 8$ K. Angle-resolved photoemission spectroscopy (ARPES) data have been measured by our group and confirms the linear band observed around the Fermi level on the surface of EuMg2Bi2. Crystals of $EuMg_2Bi_2$ can be grown easily using a conventional solid-state metal flux reaction demonstrating a more efficient pathway for achieving the TSM technology. This paper reports our recent results studied by neutron scattering, ARPES, and DFT calculations. Note, a parallel neutron scattering work was also reported on the $EuMg_2Bi_2$ system by Pakhira *et al.*[33]

EXPERIMENTAL SECTION

Synthesis

The nominal composition $EuMg_4Bi_{\sim 12}$ yielded single crystals of $EuMg_2Bi_2$ via a metal flux reaction. Reactants included elemental europium pieces (Alfa Aesar, sublimed dendritic, 99.9%), magnesium turnings (∼4 mesh, 99.98%), and bismuth pieces (99.99%). Reactants were placed in an alumina crucible and subsequently sealed in an evacuated silica tube ($<10^{-5}$ Torr) having a sample size of approximately 500 mg of stoichiometric Eu and Mg with a ∼5 g Bi metal flux. The sample was heated to 900 °C at a rate of 180 °C/h for 5 h, then cooled to 800 °C at a rate of 100 °C/h, and finally, slowly cooled to 650 °C at a rate of 3 °C/h where the samples were then centrifuged to remove the excess Bi flux. Hexagonal shaped single crystals resulted from the synthesis, and were found to be slightly oxidizing in air and moisture after one week.

Phase analysis and chemical composition determinations

A Riguku MiniFlex 600 powder x-ray diffractometer with Cu Kα radiation (λ = 1.5406 Å, Ge monochromator) and powder x-ray diffraction were employed to examine the phase identity and purity of $EuMg_2Bi_2$. A step of 0.005° and a scan speed of 1.250°/min over a Bragg angle (2θ) range of 5°–90° was analyzed. A full-profile LeBail refinement to determine phase identification and refinement of lattice parameters was performed using FullProf Suite.[34,35]

Structure and chemical composition determination

The room-temperature crystal structure of $EuMg_2Bi_2$ was determined from a Bruker Apex II single crystal x-ray diffractometer equipped with Mo radiation ($\lambda_{K\alpha} = 0.71073$ Å) using single crystals from the nominal composition $EuMg_4Bi_{\sim 12}$. The sample was measured with an ω of 0.5° per scan and an exposure time of 10 s per frame. Subsequently, the crystal structure was solved using a SHELXTL package with the direct methods and full-matrix least squares on the F^2 model.[36,37] Chemical stoichiometry was analyzed using an FEI quanta 3D Field Emission Gun (FEG) Focused Ion Beam (FIB)/Scanning Electron Microscope (SEM) and Energy-Dispersive Spectroscopy (EDS). With a 20 kV accelerating voltage, various areas from a $EuMg_2Bi_2$ crystal were selected for the spectrum collection.

Physical property measurements

A quantum design physical property measurement system (PPMS) including a temperature range of 1.85–300 K and applied

fields up to 9 T was employed for the temperature and field-dependent magnetization, resistivity, and magnetoresistivity measurements. Field-dependent and temperature-dependent magnetization measurements were performed perpendicular and parallel to the *c* axis. Normal electronic transport measurements were performed with a four-probe method using platinum wires in the basal plane of a single crystal.

Single crystal neutron diffraction

The magnetic structure of $EuMg_2Bi_2$ was determined using single crystal neutron diffraction on the Dimensional Extreme Magnetic Neutron Diffractometer (DEMAND, HB-3A) at the High Flux Isotope Reactor (HFIR) at Oak Ridge National Laboratory (ORNL).[38] A small single crystal of $EuMg_2Bi_2$ (approximately $1.2 \times 1.2 \times 0.2\ mm^3$) was selected for the measurement as a result of the large neutron absorption coefficient of Eu. The sample was measured at 4 and 10 K using neutrons with the short wavelength of 1.008 Å from the bent Si-331 monochromator to reduce the heavy neutron absorption. PLATON software was utilized to apply the absorption corrections while FullProf refinement Suite was used to perform the nuclear and magnetic structure refinements.[34,39,40]

Electronic structure calculations

Bulk band structure calculations were calculated using the generalized gradient approximation (GGA) and correlation parameter (U) with and without spin–orbit coupling (SOC) and were performed with VASP.[41] The experimental structural parameters from both x-ray and neutron diffractions were used here. Spin–orbit coupling (SOC) was included self-consistently to examine the SOC effects on the electronic and magnetic structures. Spin polarization on Eu atoms using GGA + U (U = 6 eV) was set to investigate the magnetic models.[42] Different U parameters were tested to match with the experimental ARPES measurements on Eu atoms. The Monkhorst–Pack *k*-point mesh in the Brillouin zone was set as $11 \times 11 \times 7$ for the *k*-space integrations.[43] The converged energy was set up as 0.1 meV per atom.

Experimental band structure characterization

Photoemission (ARPES) maps were obtained at the Electron Spectro-Microscopy (ESM) beamline of the National Synchrotron Light Source (NSLS-II) using a two-dimensional momentum space mapping analyzer Scienta DA30 set at angular and energy resolutions of <0.2° and 15 meV. The samples were glued to a cryostat, cooled to 10 K in ultrahigh vacuum, and cleaved prior to measurements, which resulted in flat, shiny (001) surfaces. Photon energies were in the range 60–100 eV.

RESULTS AND DISCUSSIONS

Crystal structure

Single crystal x-ray diffraction confirmed that the crystal structure of $EuMg_2Bi_2$ crystallizes into the tetragonal $CaAl_2Si_2$ structure type with space group *P*-3m1 (No. 164). Table I lists the lattice parameters of $EuMg_2Bi_2$, while Table II gives the atomic coordinates and the equivalent isotropic displacement parameters. Atomic site disorders for Eu and Bi have been refined but not observed. The structure consists of alternating Eu^{2+} and $MgBi_4$ edge-sharing tetrahedron layers. In Fig. 1(b), an image of the alternating layers can be observed, additionally, Fig. 1(a) displays the top view along the *c* axis showing the double stacked puckered Mg_3Bi_3 honeycombs. Three of the bond lengths found in the $MgBi_4$ tetrahedron share the same length of 2.914(3) Å, while the remaining Mg–Bi bond length is slightly longer at 2.965(7) Å, which is likely considering the bulky adjacent Mg^{2+} atoms. The bond angles in the $MgBi_4$ tetrahedron are all approximately equivalent at ∼109°, making this a relatively ideal tetrahedron environment. The tetragonal structure of $EuMg_2Bi_2$ is analogous to the well-established topological semimetal Mg_2Bi_3, except Eu^{2+} now replaces the Mg^{2+} layer in Mg_3Bi_2.[30] The chemical formula as determined by SEM-EDS and was found to be $Eu_{1.4(2)}Mg_{1.9(4)}Bi_{2.0(2)}$, which further verifies the chemical composition and stoichiometry of the $EuMg_2Bi_2$ phase.

TABLE I. Single crystal refinement data for $EuMg_2Bi_2$.

Refined formula	$EuMg_2Bi_2$
FW (g/mol)	618.54
Space group, Z	*P*-3m, 1
a (Å)	4.764(1)
c (Å)	7.855(2)
V (Å^3)	154.42(8)
Extinction coefficient	0.008(1)
θ range (deg)	2.593–33.198
No. reflections, R_{int}	2172, 0.0750
No. independent reflections	262
No. parameters	10
R_1, ωR_2 [$I > 2\delta(I)$]	0.0273, 0.0563
Goodness of fit	1.072
Diffraction peak and hole (e$^-$/Å^3)	1.930, −3.989

Magnetic properties of $EuMg_2Bi_2$

Multiple techniques have been used to understand the magnetic and electronic properties of $EuMg_2Bi_2$. Field-dependent magnetization curves up to 9 T were measured from 2 to 100 K with applied fields perpendicular and parallel to the *c* axis to verify with previously reported measurements, as seen in Fig. 2(a).[32] Based on the apparent magnetic saturation (MH-curve) at 2 K, the saturated magnetic moment, μ_{sat}, is approximately 7.7 μ_B/Eu^{2+}, which is in good agreement with the theoretical 7.94 μ_B per Eu^{2+} ion.

TABLE II. Atomic coordinates and equivalent isotropic displacement parameters for $EuMg_2Bi_2$ determined from the single crystal x-ray diffraction [U_{eq} is defined as one-third of the trace of the orthogonalized U_{ij} tensor (Å^2)].

Atom $EuMg_2Bi_2$	Wyck	*x*	*y*	*z*	Occ.	U_{eq}
Bi	2*d*	⅓	⅔	0.249 99(8)	1	0.012(1)
Eu	1*a*	0	0	0	1	0.015(1)
Mg	2*d*	⅓	⅔	0.627 4(8)	1	0.015(1)

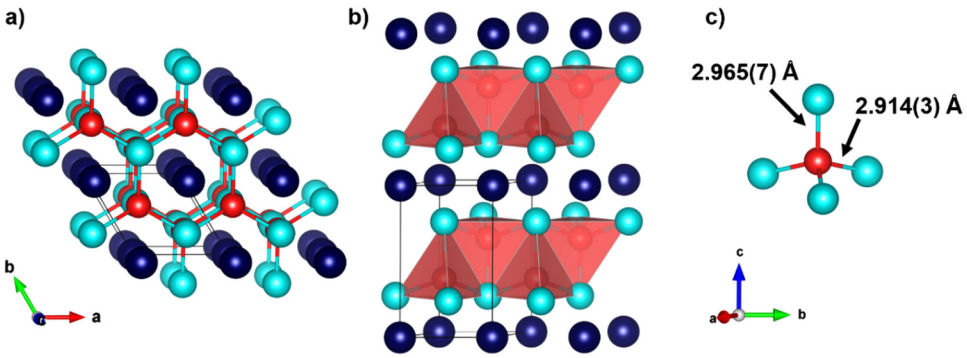

FIG. 1. Crystal structure of $EuMg_2Bi_2$. (a) The double stacked puckered Mg_3Bi_3 looking down the *c* axis, (b) the $MgBi_4$ tetrahedron from the *b*/*c*-plane, and (c) the atomic distances within the $MgBi_4$ tetrahedron.

A slight magnetic anisotropy is observed and is most prominent at 2 K, where the magnetic moment saturates at ~3 T for fields perpendicular to the *c* axis and ~3.4 T for fields parallel to the *c* axis. To further verify the magnetic behavior of $EuMg_2Bi_2$ temperature-dependent magnetic susceptibility, measurements were performed from 1.8 to 300 K at applied fields from 0.05 to 0.3 T both perpendicular and parallel to the *c* axis. As shown in Fig. 2(b), the sharp peaks at lower temperatures confirm the Néel temperatures of $EuMg_2Bi_2$, $T_{N//C} \sim 7.0$ K and $T_{N\perp C} \sim 6.7$ K. The magnetic susceptibility was fit using the modified Curie–Weiss formula, $\chi = \chi_0 + \frac{C}{T-\theta}$, where θ is the paramagnetic Curie temperature and C is the Curie constant. The resulting Curie–Weiss temperatures and effective magnetic moments were determined to be $\theta_{CW} \sim 7.4(9)$ K and $\mu_{eff} \sim 7.8(4)\ \mu_B/Eu^{2+}$ for fields perpendicular to the *c* axis and $\theta_{CW} \sim 5.5(6)$ K and $\mu_{eff} \sim 7.9(3)\ \mu_B/Eu^{2+}$ for fields parallel to the *c* axis. The observed positive θ_{CW} temperature indicates that the magnetism of $EuMg_2Bi_2$ is dominated by ferromagnetic interactions.

Electronic properties of $EuMg_2Bi_2$

The four-probe temperature and field-dependent resistivity measurements were performed in the *ab*-plane of a single crystal of $EuMg_2Bi_2$. As shown in Fig. 3(a), the temperature-dependent resistivity increases in resistivity from $\sim 1.82 \times 10^{-5}$ Ωm to $\sim 2 \times 10^{-5}$ Ωm over a temperature range of 1.8–300 K, in the absence of an applied magnetic field. This result confirms the semi-metallic behavior of $EuMg_2Bi_2$.[8] Additionally, the temperature-dependent resistivity plot reaches a minimum at ~20 K, then the resistivity increases slightly and finally proceeds to decrease. This jump at ~8.6 K can be related to the AFM ordering temperature $T_{N//C} \sim 7$ K and $T_{N\perp C} \sim 6.7$ K. The observed minimum in the resistivity has been attributed to the Anderson localization, an interference phenomenon caused by a high enough disorder in the lattice and resulting in a localized electron wavefunction.[32] In the case of $EuMg_2Bi_2$, the disorder has been potentially linked to the low carrier-density metal. A domelike feature is observed in the field-dependent resistivity and magnetoresistivity (MR) of $EuMg_2Bi_2$

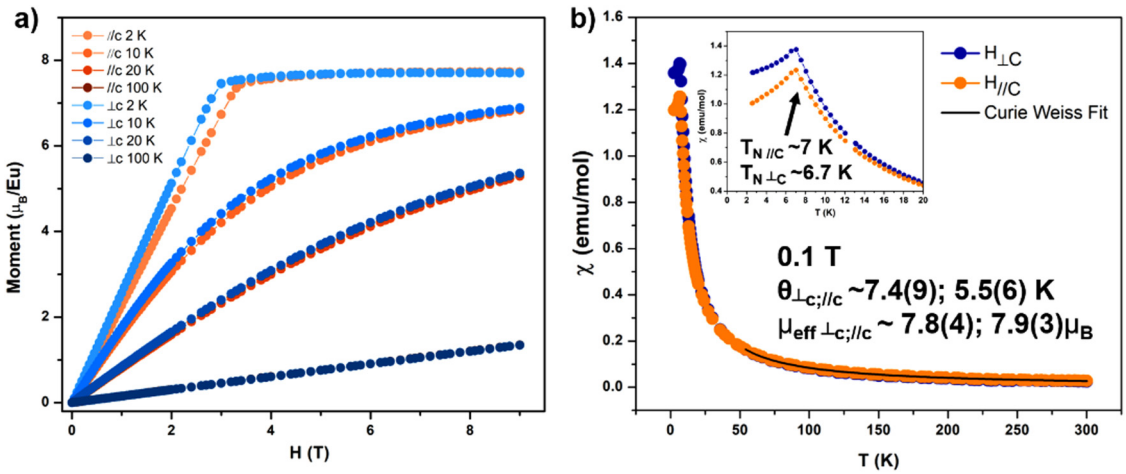

FIG. 2. (a) Magnetization curves over the temperature range 2–100 K with applied fields perpendicular (blue gradient) and parallel (orange gradient) to the *c* axis. (b) Magnetic susceptibility (χ) plots with the applied magnetic field of 0.05 T both perpendicular and parallel to the *c* axis fitted using the Curie–Weiss law (black line) at temperatures above 50 K. The small inset depicts a close-up view of the AFM transition $T_{N/C} \sim 7$ K and $T_{N\perp C} \sim 6.7$ K.

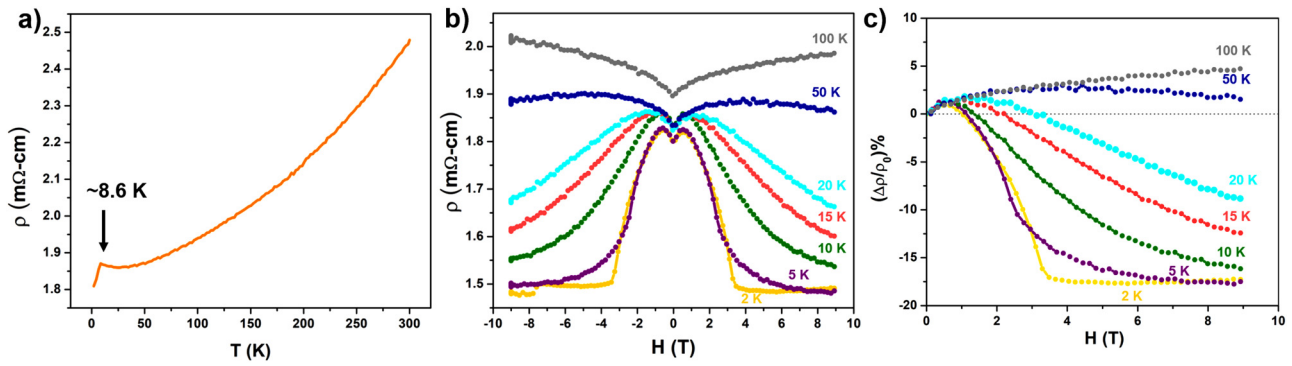

FIG. 3. Resistivity measurements of $EuMg_2Bi_2$. (a) Resistivity vs temperature from 2 to 300 K parallel to the *ab*-plane without an external magnetic field. (b) Field-dependent resistivity parallel to the *ab*-plane measurements at temperatures ranging from 2 to 100 K and (c) the magnetoresistivity plots from 2 to 100 K.

when an external magnetic field is applied parallel to the *ab*-plane, reminiscent of the proposed magnetic topological candidates $EuBiTe_3$[44] and $EuIn_2As_2$.[45] At 2 K, the MR appears to saturate at ~3 T consistent with the field-dependent magnetization plot at 2 K. The evolution of the MR with temperature can be seen in Fig. 3(c), where it transitions from largely negative ~≤20 K to slightly positive ~≥50 K. In theory,[46] the behavior of the MR for an AFM metal will either positively vary with H^2 when the applied magnetic field is along the easy axis or be negligible when the applied magnetic field is perpendicular to the easy axis. However, as can be seen in Fig. 3(c), this is clearly inconsistent with the MR for $EuMg_2Bi_2$. For this circumstance, the MR behavior may be explained by the crossover between weak localization (WL) and weak antilocalization (WAL) in terms of the competition between the AFM and FM orders, which has been speculated for previously reported materials in this family such as $EuIn_2As_2$.[44,45] Taking into account the positive Curie–Weiss temperature, which indicates the presence of a FM interaction, and the aligned in plane Eu magnetic moments determined from neutron diffraction, this kind of behavior is likely. Additionally, the high spin state of Eu^{2+} is verified in $EuMg_2Bi_2$ by the effective moment of μ_{eff} ~ 7.8(4) μ_B/Eu^{2+} and μ_{eff} ~ 7.9(3) μ_B/Eu^{2+} for fields perpendicular and parallel to the *c* axis from the temperature-dependent magnetization measurements, which suggests highly localized spins.[45] Therefore, at lower fields (≤1 T), the positive MR can originate from localized carriers that result from the long-range AFM order. While at higher fields, magnetic polarons (MP), or FM clusters, can form resulting from the large exchange interaction between localized spins and conduction electrons, giving rise to more itinerant carriers and causing the MR to decrease.[47,48] This can be observed at temperatures much higher than T_N. However, further investigations should be performed in order to fully understand the magnetoresistivity behavior in $EuMg_2Bi_2$. An extensive discussion on the electronic transport properties of $EuMg_2Bi_2$ has been provided by Pakhira *et al.*.[32]

A-type magnetic structure of $EuMg_2Bi_2$

Based on the neutron single crystal diffraction experiment measured on the HB-3A Dimensional Extreme Magnetic Neutron Diffractometer (DEMAND), it was found that a set of magnetic peaks at 4 K can be reasonably indexed by the k vector (0, 0, ½), as shown in Fig. 4. Due to the heavy absorbance of Eu in $EuMg_2Bi_2$, we used the shortest available wavelength to reduce the absorption effect. The absorption correction was carefully taken by using PLATON software.[39,40] At 4 K, the spins align ferromagnetically within the *ab* plane, which can potentially explain the observed positive θ_{CW} determined from the bulk measurements; however, the antiferromagnetic spin alignment between the Eu layers [see Fig. 4(c)] is consistent with the antiferromagnetic transition observed in the bulk magnetic susceptibility data. Note, the magnetic structure is also consistent with the recently reported magnetic structure for $EuMg_2Bi_2$ by Pakhira *et al.*[33] This magnetic structure is similar to $EuSn_2P_2$,[15] another potential magnetic topological Eu based 122 material discovered by our group. The resulting refined magnetic moment at 4 K was 6.610(37) μ_B/Eu, which is lower than the expected theoretical total magnetic moment of 7.94 μ_B per Eu^{2+} ion. Additionally, the refined magnetic moment reported here is slightly higher than the recently reported magnetic moment of 5.3(5) μ_B/Eu.[33] The temperature dependence of the magnetic scattering at (0 0 2.5) may follow the empirical power law $I = A(T_M - T/T_M)^{2\beta} + B$, where T_M is the magnetic phase transition critical temperature, A is the proportionality constant, β is the order parameter critical exponent, and B is the background. The best fit was performed in the temperature range ~5.2–8 K, shown as the red line in Fig. 4(a), which revealed a magnetic transition temperature of T_M ~ 6.72(7) K. As a result of the limited neutron scattering data, an accurate interpretation of the power law fitting could not be attained while allowing for all free variables, thus the β value was fixed. Considering the most desirable fitting was achieved with a fixed β value of 0.23, this system can be described by the 2D Heisenberg model, which is consistent with the weak interlayer antiferromagnetic coupling suggested by the well matched positive CW temperature and T_N (i.e., FM is the dominant interaction and the AFM interaction is negligible). From the power law, the calculated magnetic moment at T = 0 K was determined to be 6.79(4) μ_B/Eu, indicating that the magnetic moment continues to order past 4 K. This may help us to explain the tendency of the ordering parameter to saturate at lower temperatures, as shown in Fig. 4(a).

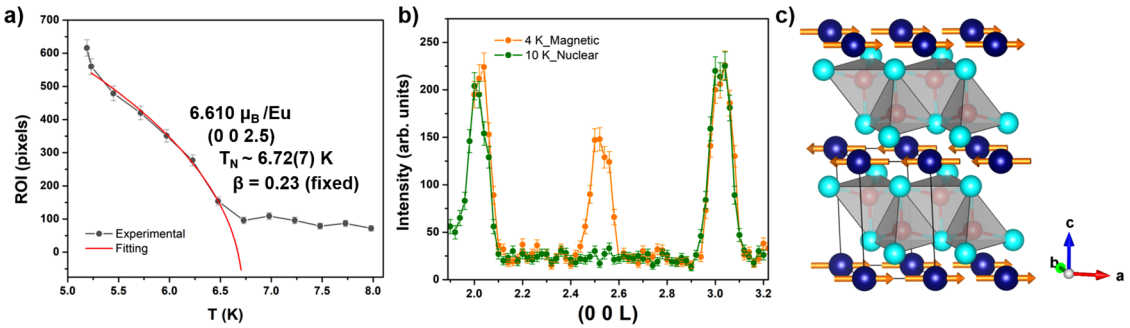

FIG. 4. Neutron scattering measurements of $EuMg_2Bi_2$. (a) Temperature dependence of the magnetic scattering at (0 0 2.5) for $EuMg_2Bi_2$ indicating a TN ~ 6.72(7) K. The red line represents the fitting of the power law. (b) Diffraction intensity vs (0 0 L) at 4 and 10 K comparing the magnetic and nuclear peaks of $EuMg_2Bi_2$. (c) Magnetic structure of $EuMg_2Bi_2$ along the *c* axis.

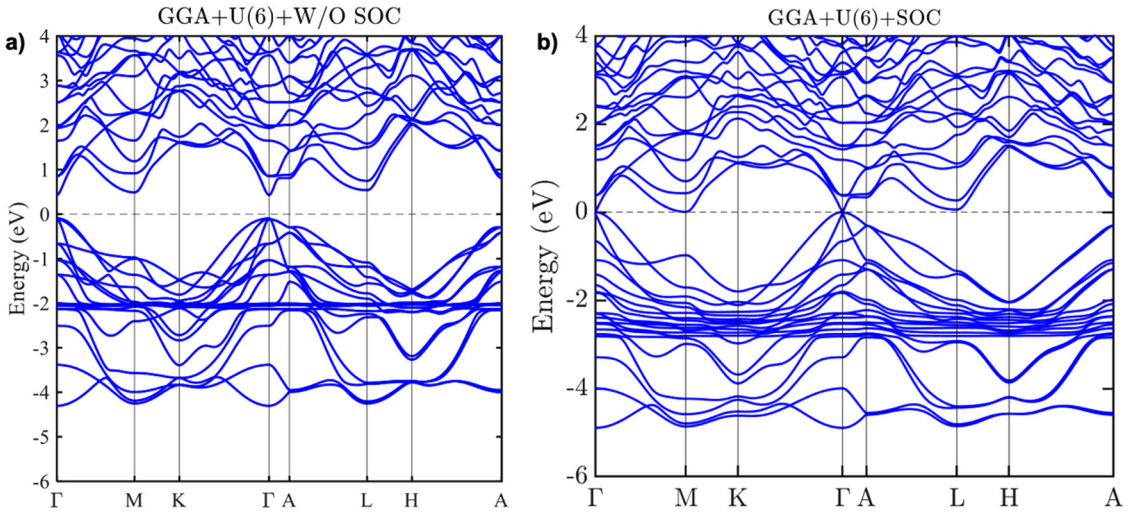

FIG. 5. Bulk band structure calculations using LDA for $EuMg_2Bi_2$. Surface band structure calculations using generalized gradient approximation (GGA), (a) U = 6 eV without SOC, (b) U = 6 eV with SOC.

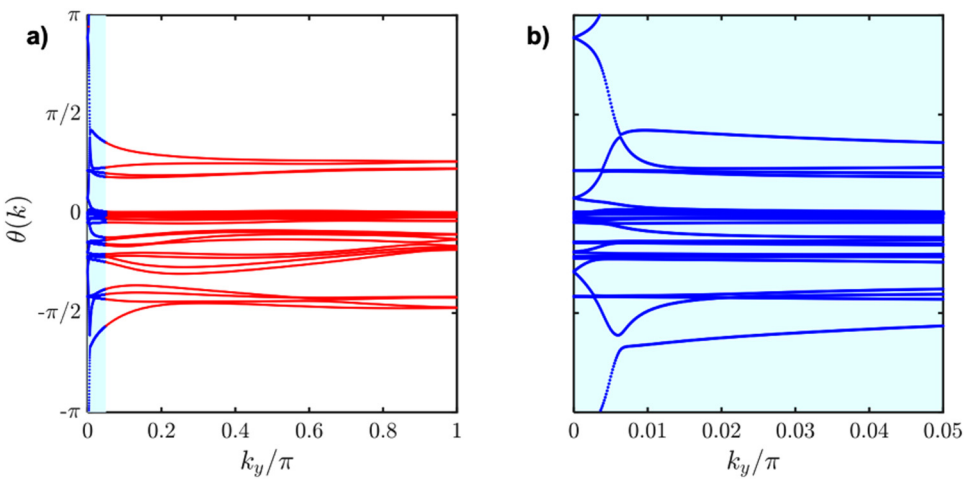

FIG. 6. Calculated Z_2 topological invariant for $EuMg_2Bi_2$ shown for the time reversal invariant planes between π and −π.

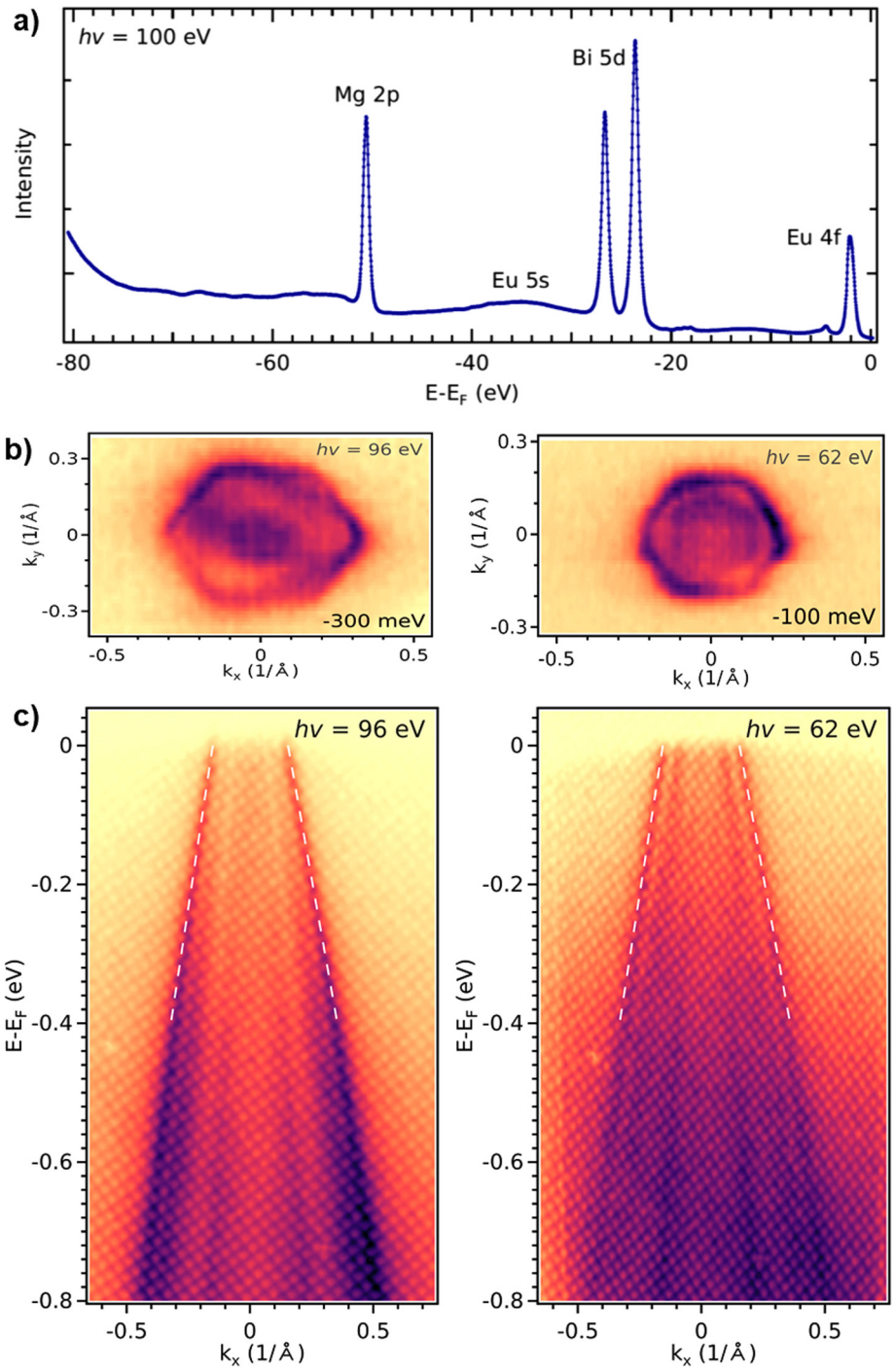

FIG. 7. Angle-resolved photoemission data for the electronic structure of $EuMg_2Bi_2$. Momentum k_x is along the M–Γ–M direction of the hexagonal surface Brillouin zone. (a) Core level spectrum at hν = 100 eV showing the characteristic double peak of Bi 5*d*, and peaks of Mg 2*p* and Eu 4*f* with low intensity contributions of Eu 5*s* and Eu 5*p*. (b) Constant energy plots of the band structure around Γ at −100 meV (using hν = 62 eV) and −300 meV (using hν = 96 eV) with respect to the Fermi level. (c) Band dispersion at two different perpendicular momenta. The same pair of dashed lines is shown on top of both spectra. The outer bands are most likely surface states.

Electronic structure of $EuMg_2Bi_2$

To understand the magnetic and electronic properties of $EuMg_2Bi_2$, electronic structure calculations were performed using the generalized gradient approximation (GGA) plus a correlation parameter U of 6 for both with and without spin–orbit coupling (SOC), as shown in Fig. 5. A small continuous bandgap of ∼0.4 eV is seen throughout the Brillouin zone without SOC, which has been previously attributed to the large hole mobility in $EuMg_2Bi_2$ and the strong hybridization between Bi and Eu atoms.[49-51] The Eu 4*f* electrons are roughly localized around −2 without SOC and in

between −2 and −3 with SOC. The Mg and Bi states are hybridized and located near the Fermi level. The calculated magnetic moment on the Eu atoms was determined to be 7 $\mu_{B,}$ which is consistent with the bulk magnetic measurements. Considering the GGA + U with SOC, the small bandgap disappears, and Fermi surface states appear around the Γ points.

The Z2 topological invariant was calculated by the Wilson loop method in Fig. 6. The Wilson band is an open curve traversing the entire Brillouin zone in the time reversal invariant plane $kz = 0$. The result shows that the $Z2$ invariant equals 1, indicating that $EuMg_2Bi_2$ is a good topological insulator in the presence of SOC.

Electronic structure measurement by ARPES

The core level photoemission spectrum presented in Fig. 7(a) exhibits two characteristic high-intensity peaks of Bi 5*d* orbitals, and sharp peaks of Mg 2*p* and Eu 4*f*. This confirms the chemical composition of our samples, and the cleaved surface purity. ARPES maps taken at 10 K from the (001) surface, which is the surface at which $EuMg_2Bi_2$ naturally cleaves, show several hole-like bands encircling the Γ point of the surface Brillouin zone. The outer band, consistently the sharpest and most intense at all photon energies, exhibits hexagonal constant energy contours, consistent with the threefold symmetry of the material. Inside of the contour, at least two other distinct bands are present at the binding energies probed; their shape and visibility change with photon energies, which signifies different cuts of the bulk band structure at different perpendicular momenta. The outer band, as can be seen from our spectra along M–Γ–M at photon energies of 62 and 96 eV, Fig. 7(c), shows no measurable perpendicular momentum dependence. Namely, as these photon energies represent approximately a 0.95 1/Å change of kz, which is 2.4 times π/c, the spectra are guaranteed to come from different parts of the Brillouin zone; yet, the measured bands under the same pair of dashed lines added in Fig. 3(c) do not change position. Unsurprisingly, this band is similar to that observed in structurally related type-II nodal-line semimetal Mg_3Bi_2.[25] All bands appear highly linear, dispersing at 2.5×10^5 m/s. Our results differ from a recent unpublished study by Kabir *et al.*[29] Inasmuch as our core level spectra show all the expected peaks, our surface Brillouin zone is hexagonal and not square, and the only bands crossing the Fermi level are those around Γ.

CONCLUSION

After refinement of the neutron scattering data including an applied absorption correction, the A-type magnetic structure of $EuMg_2Bi_2$ was revealed. Similar to other materials in the Eu based 122 family, the Eu^{2+} moments in $EuMg_2Bi_2$ are ferromagnetically ordered in the plane and antiferromagnetically stacked along the c axis. The bulk magnetic susceptibility measurements indicated a dominant FM interaction from the positive Curie–Weiss temperatures of $\theta_{CW} \sim 7.4(9)$ K and $\theta_{CW} \sim 5.5(6)$ K for fields perpendicular and parallel to the c axis, respectively. The reduced ordering moment of 6.61(4) μ_B/Eu is an indication of a secondary interlayer antiferromagnetic interaction. This is also consistent with the 2D Heisenberg model that well fits the magnetic ordering parameter. Likewise, the magnetoresistivity measurements exhibit a similar dependence on the competition between the AFM and FM interactions. The resulting ARPES measurements reveal the outer linearly dispersed Dirac surface states, similar to that observed in the type-II nodal-line semimetal Mg_3Bi_2,[30] and are consistent with our experimental prediction.

SUPPLEMENTARY MATERIAL

See the supplementary material for powder x-ray diffraction data and single crystal XRD information.

ACKNOWLEDGMENTS

The work at Rutgers was supported by Beckman Young Investigator (to Weiwei Xie) and No. NSF-DMR-2053287. M.M. was supported by DOE Office of Science Graduate Student Research (SCGSR) Fellowship program. H.C. was supported by the U.S. Department of Energy (DOE), Office of Science, Office of Basic Energy Sciences, Early Career Research Program Award No. KC0402010 under Contract No. DE-AC05-00OR22725. This research used resources at the High Flux Isotope Reactor, a DOE Office of Science User Facility operated by ORNL. T.-R.C. was supported by the Young Scholar Fellowship Program from the Ministry of Science and Technology (MOST) in Taiwan under a MOST Grant for the Columbus Program No. MOST109-2636-M-006-002, National Cheng Kung University, Taiwan, and National Center for Theoretical Sciences, Taiwan. This work was supported partially by the MOST, Taiwan, Grant No. MOST107-2627-E-006-001. This research was supported, in part, by Higher Education Sprout Project, Ministry of Education to the Headquarters of University Advancement at National Cheng Kung University (NCKU).

DATA AVAILABILITY

The data that support the findings of this study are available from the corresponding authors upon reasonable request.

REFERENCES

[1]O. Vafek and A. Vishwanath, "Dirac fermions in solids—From high Tc cuprates and graphene to topological insulators and Weyl semimetals," Annu. Rev. Condens. Matter Phys. **5**, 83–112 (2014).
[2]M. Sato and Y. Ando, "Topological superconductors: A review," Rep. Prog. Phys. **80**, 076501 (2017).
[3]R. Li, J. Wang, X.-L. Qi, and S.-C. Zhang, "Dynamical axion field in topological magnetic insulators," Nat. Phys. **6**, 284–288 (2010).
[4]A. M. Essin, J. E. Moore, and D. Vanderbilt, "Magnetoelectric polarizability and axion electrodynamics in crystalline insulators," Phys. Rev. Lett. **102**, 146805 (2009).
[5]C.-Z. Chang, J. Zhang, X. Feng, J. Shen, Z. Zhang, M. Guo, K. Li, Y. Ou, P. Wei, L.-L. Wang, Z.-Q. Ji, Y. Feng, S. Ji, X. Chen, J. Jia, X. Dai, Z. Fang, S.-C. Zhang, K. He, Y. Wang, L. Lu, X.-C. Ma, and Q.-K. Xue, "Experimental observation of the quantum anomalous Hall effect in a magnetic topological insulator," Science **340**, 167–170 (2013).
[6]X.-L. Qi, T. L. Hughes, and S.-C. Zhang, "Chiral topological superconductor from the quantum Hall state," Phys. Rev. B **82**, 184516 (2010).
[7]L. M. Schoop, X. Dai, R. J. Cava, and R. Ilan, "Special topic on topological semimetals—New directions," APL Mater. **8**, 030401 (2020).
[8]A. F. May, M. A. McGuire, J. Ma, O. Delaire, A. Huq, D. J. Singh, W. Cai, and H. Wang, "Thermoelectric transport properties of $CaMg_2Bi_2$, $EuMg_2Bi_2$, and $YbMg_2Bi_2$," Phys. Rev. B **85**, 035202 (2012).

[9]J. Lim, Y. S. Ang, F. J. García de Abajo, I. Kaminer, L. K. Ang, and L. J. Wong, "Efficient generation of extreme terahertz harmonics in three-dimensional Dirac semimetals," Phys. Rev. Res. **2**, 043252 (2020).
[10]K. J. A. Ooi, Y. S. Ang, Q. Zhai, D. T. H. Tan, L. K. Ang, and C. K. Ong, "Nonlinear plasmonics of three-dimensional Dirac semimetals," APL Photonics **4**, 034402 (2018).
[11]O. F. Shoron, M. Goyal, B. Guo, D. A. Kealhofer, T. Schumann, and S. Stemmer, "Prospects of terahertz transistors with the topological semimetal cadmium arsenide," Adv. Electron. Mater. **6**, 2000676 (2020).
[12]L. Cao, G. Zhou, Q. Wu, S. A. Yang, H. Y. Yang, Y. S. Ang, and L. K. Ang, "Electrical contact between an ultrathin topological Dirac semimetal and a two-dimensional material," Phys. Rev. Appl. **13**, 054030 (2020).
[13]Topological semimetal nanostructures, from properties to topotronics, see https://pubs-acs-org.proxy.libraries.rutgers.edu/doi/full/10.1021/acsnano.9b07990 (accessed December 19, 2020)
[14]R. Yu, W. Zhang, H.-J. Zhang, S.-C. Zhang, X. Dai, and Z. Fang, "Quantized anomalous Hall effect in magnetic topological insulators," Science **329**, 61–64 (2010).
[15]X. Gui, I. Pletikosic, H. Cao, H.-J. Tien, X. Xu, R. Zhong, G. Wang, T.-R. Chang, S. Jia, T. Valla, W. Xie, and R. J. Cava, "A new magnetic topological quantum material candidate by design," ACS Cent. Sci. **5**, 900–910 (2019).
[16]S. Huang, J. Kim, W. A. Shelton, E. W. Plummer, and R. Jin, "Nontrivial Berry phase in magnetic $BaMnSb_2$ semimetal," Proc. Natl. Acad. Sci. U.S.A. **114**, 6256–6261 (2017).
[17]Z. Wang, Y. Sun, X.-Q. Chen, C. Franchini, G. Xu, H. Weng, X. Dai, and Z. Fang, "Dirac semimetal and topological phase transitions in A_3Bi (A = Na, K, Rb)," Phys. Rev. B **85**, 195320 (2012).
[18]S. K. Kushwaha, J. W. Krizan, B. E. Feldman, A. Gyenis, M. T. Randeria, J. Xiong, S.-Y. Xu, N. Alidoust, I. Belopolski, T. Liang, M. Z. Hasan, N. P. Ong, A. Yazdani, and R. J. Cava, "Bulk crystal growth and electronic characterization of the 3D Dirac semimetal Na_3Bi," APL Mater. **3**, 041504 (2015).
[19]S. Borisenko, Q. Gibson, D. Evtushinsky, V. Zabolotnyy, B. Büchner, and R. J. Cava, "Experimental realization of a three-dimensional Dirac semimetal," Phys. Rev. Lett. **113**, 027603 (2014).
[20]S. Klemenz, S. Lei, and L. M. Schoop, "Topological semimetals in square-net materials," Annu. Rev. Mater. Res. **49**, 185–206 (2019).
[21]B.-B. Fu, C.-J. Yi, T.-T. Zhang, M. Caputo, J.-Z. Ma, X. Gao, B. Q. Lv, L.-Y. Kong, Y.-B. Huang, P. Richard, M. Shi, V. N. Strocov, C. Fang, H.-M. Weng, Y.-G. Shi, T. Qian, and H. Ding, "Dirac nodal surfaces and nodal lines in ZrSiS," Sci. Adv. **5**, eaau6459 (2019).
[22]J. Park, G. Lee, F. Wolff-Fabris, Y. Y. Koh, M. J. Eom, Y. K. Kim, M. A. Farhan, Y. J. Jo, C. Kim, J. H. Shim, and J. S. Kim, "Anisotropic Dirac Fermions in a Bi square net of $SrMnBi_2$," Phys. Rev. Lett. **107**, 126402 (2011).
[23]X. Zhang, Q. Liu, Q. Xu, X. Dai, and A. Zunger, "Topological insulators versus topological Dirac semimetals in honeycomb compounds," J. Am. Chem. Soc. **140**, 13687–13694 (2018).
[24]A. F. May, M. A. McGuire, and B. C. Sales, "Effect of Eu magnetism on the electronic properties of the candidate Dirac material $EuMnBi_2$," Phys. Rev. B **90**, 075109 (2014).
[25]H. Masuda, H. Sakai, M. Tokunaga, Y. Yamasaki, A. Miyake, J. Shiogai, S. Nakamura, S. Awaji, A. Tsukazaki, H. Nakao, Y. Murakami, T. Arima, Y. Tokura, and S. Ishiwata, "Quantum Hall effect in a bulk antiferromagnet $EuMnBi_2$ with magnetically confined two-dimensional dirac fermions," Sci. Adv. **2**, e1501117 (2016).
[26]Y. Shiomi, H. Watanabe, H. Masuda, H. Takahashi, Y. Yanase, and S. Ishiwata, "Observation of magnetopiezoelectric effect in antiferromagnetic metal $EuMnBi_2$," Phys. Rev. Lett. **122**, 127207 (2019).
[27]S. Borisenko, D. Evtushinsky, Q. Gibson, A. Yaresko, K. Koepernik, T. Kim, M. Ali, J. van den Brink, M. Hoesch, A. Fedorov, E. Haubold, Y. Kushnirenko, I. Soldatov, R. Schäfer, and R. J. Cava, "Time-reversal symmetry breaking type-II Weyl state in $YbMnBi_2$," Nat. Commun. **10**, 3424 (2019).
[28]J.-R. Soh, H. Jacobsen, B. Ouladdiaf, A. Ivanov, A. Piovano, T. Tejsner, Z. Feng, H. Wang, H. Su, Y. Guo, Y. Shi, and A. T. Boothroyd, "Magnetic structure and excitations of the topological semimetal $YbMnBi_2$," Phys. Rev. B **100**, 144431 (2019).
[29]N. H. Jo, B. Kuthanazhi, Y. Wu, E. Timmons, T.-H. Kim, L. Zhou, L.-L. Wang, B. G. Ueland, A. Palasyuk, D. H. Ryan, R. J. McQueeney, K. Lee, B. Schrunk, A. A. Burkov, R. Prozorov, S. L. Bud'ko, A. Kaminski, and P. C. Canfield, "Manipulating of magnetism in the topological semimetal $EuCd_2As_2$," Phys. Rev. B **101**, 140402 (2020).
[30]T.-R. Chang, I. Pletikosic, T. Kong, G. Bian, A. Huang, J. Denlinger, S. K. Kushwaha, B. Sinkovic, H.-T. Jeng, T. Valla, W. Xie, and R. J. Cava, "Realization of a type-II nodal-line semimetal in Mg_3Bi_2," Adv. Sci. **6**, 1800897 (2019).
[31]A. F. May, M. A. McGuire, D. J. Singh, R. Custelcean, and G. E. Jellison, "Structure and properties of single crystalline $CaMg_2Bi_2$, $EuMg_2Bi_2$, and $YbMg_2Bi_2$," Inorg. Chem. **50**, 11127–11133 (2011).
[32]S. Pakhira, M. A. Tanatar, and D. C. Johnston, "Magnetic, thermal, and electronic-transport properties of $EuMg_2Bi_2$ single crystals," Phys. Rev. B **101**, 214407 (2020).
[33]S. Pakhira, T. Heitmann, S.X.M. Riberolles, B.G. Ueland, R.J. McQueeney, D.C. Johnston, and D. Vaknin, Zero-field magnetic ground state of $EuMg_2Bi_2$, http://arxiv.org/abs/2009.06880 (2020) (accessed October 20, 2020).
[34]J. Rodríguez-Carvajal, "Recent advances in magnetic structure determination by neutron powder diffraction," Phys. B Condens. Matter **192**, 55–69 (1993).
[35]R. E. Dinnebier and S. J. L. Billinge, "Chapter 1: Principles of powder diffraction," in *Powder Diffraction: Theory and Practice* (RSC Publishing, 2008), pp. 1–19. doi:10.1039/9781847558237-00001
[36]G. M. Sheldrick, "Crystal structure refinement with SHELXL," Acta Crystallogr. Sect. C Struct. Chem. **71**, 3–8 (2015).
[37]G. M. Sheldrick, "SHELXT—Integrated space-group and crystal-structure determination," Acta Crystallogr. Sect. Found. Adv. **71**, 3–8 (2015).
[38]H. Cao, B. C. Chakoumakos, K. M. Andrews, Y. Wu, R. A. Riedel, J. Hodges, W. Zhou, R. Gregory, B. Haberl, J. Molaison, and G. W. Lynn, "DEMAND, a dimensional extreme magnetic neutron diffractometer at the high flux isotope reactor," Crystals **9**, 5 (2019).
[39]A. L. Spek, "Single-crystal structure validation with the program PLATON," J. Appl. Crystallogr. **36**, 7–13 (2003).
[40]A. L. Spek, "PLATON SQUEEZE: A tool for the calculation of the disordered solvent contribution to the calculated structure factors," Acta Crystallogr. Sect. C Struct. Chem. **71**, 9–18 (2015).
[41]J. P. Perdew, K. Burke, and M. Ernzerhof, "Generalized gradient approximation made simple," Phys. Rev. Lett. **77**, 3865–3868 (1996).
[42]J. P. Dahl and J. Avery, *Local Density Approximations in Quantum Chemistry and Solid State Physics* (Springer Science & Business Media, 2013)
[43]H. J. Monkhorst and J. D. Pack, "Special points for Brillouin-zone integrations," Phys. Rev. B **13**, 5188–5192 (1976).
[44]W. Shon, J.-S. Rhyee, Y. Jin, and S.-J. Kim, "Magnetic polaron and unconventional magnetotransport properties of the single-crystalline compound $EuBiTe_3$," Phys. Rev. B **100**, 024433 (2019).
[45]Y. Zhang, K. Deng, X. Zhang, M. Wang, Y. Wang, C. Liu, J.-W. Mei, S. Kumar, E. F. Schwier, K. Shimada, C. Chen, and B. Shen, "In-plane antiferromagnetic moments and magnetic polaron in the axion topological insulator candidate $EuIn_2As_2$," Phys. Rev. B **101**, 205126 (2020).
[46]H. Yamada and S. Takada, "Magnetoresistance of antiferromagnetic metals Due to s-d interaction," J. Phys. Soc. Jpn. **34**, 51–57 (1973).
[47]P. Majumdar and P. B. Littlewood, "Dependence of magnetoresistivity on charge-carrier density in metallic ferromagnets and doped magnetic semiconductors," Nature **395**, 479–481 (1998).
[48]M. Pohlit, S. Rößler, Y. Ohno, H. Ohno, S. von Molnár, Z. Fisk, J. Müller, and S. Wirth, "Evidence for ferromagnetic clusters in the colossal-magnetoresistance material EuB_6," Phys. Rev. Lett. **120**, 257201 (2018).
[49]M. M. Otrokov, I. I. Klimovskikh, H. Bentmann, D. Estyunin, A. Zeugner, Z. S. Aliev, S. Gaß, A. U. B. Wolter, A. V. Koroleva, A. M. Shikin, M. Blanco-Rey, M. Hoffmann, I. P. Rusinov, A. Y. Vyazovskaya, S. V. Eremeev, Y. M. Koroteev, V. M. Kuznetsov, F. Freyse, J. Sánchez-Barriga, I. R. Amiraslanov, M. B. Babanly,

N. T. Mamedov, N. A. Abdullayev, V. N. Zverev, A. Alfonsov, V. Kataev, B. Büchner, E. F. Schwier, S. Kumar, A. Kimura, L. Petaccia, G. Di Santo, R. C. Vidal, S. Schatz, K. Kißner, M. Ünzelmann, C. H. Min, S. Moser, T. R. F. Peixoto, F. Reinert, A. Ernst, P. M. Echenique, A. Isaeva, and E. V. Chulkov, "Prediction and observation of an antiferromagnetic topological insulator," Nature. **576**, 416–422 (2019).

[50]N. Mao, H. Wang, X. Hu, C. Niu, B. Huang, and Y. Dai, "Antiferromagnetic topological insulator in stable exfoliated two-dimensional materials," Phys. Rev. B **102**, 115412 (2020).

[51]T. K. Bhowmick, A. De, and R. K. Lake, "High figure of merit magneto-optics from interfacial skyrmions on topological insulators," Phys. Rev. B **98**, 024424 (2018).